Characterization of the Manganese O_2-Evolving Complex and the Iron–Quinone Acceptor Complex in Photosystem II from a Thermophilic Cyanobacterium by Electron Paramagnetic Resonance and X-ray Absorption Spectroscopy†

Ann E. McDermott,‡,§ Vittal K. Yachandra,§ R. D. Guiles,‡,§ James L. Cole,‡,§ S. L. Dexheimer,§,∥ R. D. Britt,§,∥ Kenneth Sauer,*,‡,§ and Melvin P. Klein*,§

Laboratory of Chemical Biodynamics, Lawrence Berkeley Laboratory, Department of Chemistry, and Department of Physics, University of California, Berkeley, California 94720

Received October 21, 1987; Revised Manuscript Received January 26, 1988

ABSTRACT: The Mn donor complex in the S_1 and S_2 states and the iron–quinone acceptor complex (Fe^{2+}–Q) in O_2-evolving photosystem II (PS II) preparations from a thermophilic cyanobacterium, *Synechococcus* sp., have been studied with X-ray absorption spectroscopy and electron paramagnetic resonance (EPR). Illumination of these preparations at 220–240 K results in formation of a multiline EPR signal very similar to that assigned to a Mn S_2 species observed in spinach PS II, together with $g = 1.8$ and 1.9 EPR signals similar to the Fe^{2+}–Q_A^- acceptor signals seen in spinach PS II. Illumination at 110–160 K does not produce the $g = 1.8$ or 1.9 EPR signals, nor the multiline or $g = 4.1$ EPR signals associated with the S_2 state of PS II in spinach; however, a signal which peaks at $g = 1.6$ appears. The most probable assignment of this signal is an altered configuration of the Fe^{2+}–Q_A^- complex. In addition, no donor signal was seen upon warming the 140 K illuminated sample to 215 K. Following continuous illumination at temperatures between 140 and 215 K, the average X-ray absorption Mn K-edge inflection energy changes from 6550 eV for a dark-adapted (S_1) sample to 6551 eV for the illuminated (S_2) sample. The shift in edge inflection energy indicates an oxidation of Mn, and the absolute edge inflection energies indicate an average Mn oxidation state higher than Mn(II). Upon illumination a significant change was observed in the shape of the features associated with 1s to 3d transitions. The S_1 spectrum resembles those of Mn(III) complexes, and the S_2 spectrum resembles those of Mn(IV) complexes. The extended X-ray absorption fine structure (EXAFS) spectrum of the Mn complex is similar in the S_1 and S_2 states. Simulations indicate O or N ligands at 1.75 ± 0.05 Å, transition metal neighbor(s) at 2.73 ± 0.05 Å, which are assumed to be Mn, and terminal ligands which are probably N and O at a range of distances around 2.2 Å. The Mn–O bond length of 1.75 Å and the transition metal at 2.7 Å indicate the presence of a di-μ-oxo-bridged Mn structure. Simulations indicate that a symmetric tetranuclear cluster is unlikely to be present, while binuclear, trinuclear, or highly distorted tetranuclear structures are possible. The striking similarity of these results to those from spinach PS II suggests that the structure of the Mn complex is largely conserved across evolutionarily diverse O_2-evolving photosynthetic species.

Photosystem II of cyanobacteria and higher plants consists of a reaction center quite similar to the structurally characterized reaction center of purple nonsulfur bacteria (Deisenhofer et al., 1985), together with a donor complex that extracts electrons from water. The bacterial reaction center and the reaction center of PS II[1] catalyze the light-dependent electron transfer from a specialized chlorophyll pigment to a quinone. The PS II reaction center includes two proteins called D1 and D2 which are homologous to the bacterial reaction center proteins L and M (Hearst, 1986). Like L and M, the D1 and D2 proteins bind the primary electron-donor chlorophyll species, a pheophytin acceptor (Nanba & Satoh, 1987), and two quinone electron acceptors Q_A and Q_B (Pfister et al., 1981; Worland et al., 1987). The donor complex couples the four-electron chemistry of O_2 production from H_2O to the one-electron reactions of the reaction center by serial accumulation of oxidizing equivalents such that O_2 is released on every fourth charge separation step (Joliot et al., 1969; Kok et al., 1970). The partially oxidized intermediates of the donor complex are called S states; S_1 is the principal S state of a long-term dark-adapted sample, and the S state advances by one on each charge separation of the reaction center until S_4 is produced, which converts spontaneously to form S_0 and O_2.

† This work was supported by a grant from the National Science Foundation (PCM 82-16127 and PCM 84-16676) and by the Director, Division of Energy Biosciences, Office of Basic Energy Sciences, Office of Energy Research of the Department of Energy, under Contract DE-AC03-76SF00098. Synchrotron radiation facilities were provided by the Stanford Synchrotron Radiation Laboratory which is supported by the U.S. Department of Energy, Office of Basic Energy Sciences, and the NIH Biotechnology Program, Division of Research Resources. This is paper 9 in the series "The State of Manganese in the Photosynthetic Apparatus".

* To whom correspondence should be addressed.

‡ Department of Chemistry.

§ Laboratory of Chemical Biodynamics, Lawrence Berkeley Laboratory.

∥ Department of Physics.

[1] Abbreviations: Chl, chlorophyll; DCMU, 3-(3,4-dichlorophenyl)-1,1-dimethylurea; DCBQ, 2,6-dichloro-*p*-benzoquinone; EDTA, ethylenediaminetetraacetic acid; EPR, electron paramagnetic resonance; ESE-NEM, electron spin-echo nuclear envelope modulation; EXAFS, extended X-ray absorption fine structure; Fe^{2+}–Q, iron–quinone acceptor complex; HEPES, *N*-(2-hydroxyethyl)piperazine-*N*′-2-ethanesulfonic acid; MES, 4-morpholineethanesulfonic acid; MLS, multiline EPR signal associated with the S_2 state of PS II; PMS, *N*-methylphenazonium methosulfate; PMSF, phenylmethanesulfonyl fluoride; PS I, photosystem I; PS II, photosystem II; P700, photosystem I reaction center chlorophyll; Q_A and Q_B, quinone electron acceptors in the reaction center of purple nonsulfur bacteria and PS II; Tris, tris(hydroxymethyl)aminomethane; XAS, X-ray absorption spectroscopy.

0006-2960/88/0427-4021$01.50/0

In contrast to the products of serial one-electron oxidation of H_2O to O_2, S_1 is very stable, and S_2 and S_3 are stable on the time scale of a few minutes (Renger, 1978; Sauer, 1980). A protein-bound Mn complex is thought to be the catalyst for H_2O oxidation. A point mutation in the D1 polypeptide interferes with Mn binding, suggesting that D1 may provide ligands for the Mn complex (Metz et al., 1986). The detailed structure and chemistry of this catalyst are of obvious importance but have remained difficult to uncover.

A picture has emerged from EPR and X-ray absorption studies of PS II from spinach in which the Mn catalyst is a cluster containing two to four Mn atoms which are primarily Mn(III) and/or Mn(IV). The first spectroscopic signature of Mn associated with an S state arose from the S_2 state and was an EPR signal centered at $g = 2$ with 16–19 hyperfine lines, called the multiline signal (Dismukes & Siderer, 1980). This signal is similar to the EPR spectra of a variety of Mn_2 (III/IV) complexes with $S = {}^1/_2$ ground states (Cooper et al., 1978; Plaksin et al., 1972; Sheats et al., 1987). A second EPR signal at $g = 4.1$ was subsequently discovered (Casey & Sauer, 1984) and assigned as a Mn species in the S_2 state (Zimmermann & Rutherford, 1986; Cole et al., 1987a). This signal resembles EPR spectra from the $S = {}^3/_2$ state of axially distorted Mn(IV) monomeric inorganic complexes (Lynch et al., 1984; Magers et al., 1980; Richens & Sawyer, 1979). ESE-NEM studies of the multiline signal indicated little modulation by N ligands, suggesting mostly O ligands for Mn (Britt et al., 1987). EXAFS and X-ray absorption edge studies of Mn in PS II from spinach indicate (1) a μ-oxo-bridged Mn complex that is not likely to be a symmetric tetranuclear cluster, (2) an average valence between Mn(III) and Mn(IV), (3) an oxidation of Mn by 1–2 equiv per reaction center in the S_1 to S_2 transition, which confirmed a redox role for Mn in water oxidation, and (4) no apparent change in structure in the S_1 to S_2 transition (Yachandra et al., 1986, 1987).

Along with PS I, PS II reaction centers are present in a variety of organisms, including higher plants, which appeared approximately 10^8 years ago, and the prokaryotic cyanobacteria, which probably appeared 2.5×10^9 years ago and which are thought to resemble the first O_2-evolving organisms on earth (Schopf, 1978; Valentine, 1978). Although most spectroscopic studies of Mn in PS II have focused on the more easily prepared spinach PS II, in many respects it is more useful to work with prokaryotic organisms. For example, isotopic labeling and site-specific genetic modifications provide useful techniques for studies of ligand identity and are most conveniently done with a prokaryote. Differences in the proteins of the donor complex between eukaryotic and prokaryotic organisms have been reported, including (1) the lack of 24- and 18-kDa proteins in cyanobacteria (Stewart et al., 1985) which in spinach PS II stabilize binding of two necessary cofactors of O_2 evolution, Ca^{2+} and Cl^- (Ghanotakis & Yocum, 1985), (2) different salt extraction properties of a 33-kDa protein (Koike & Inoue, 1985) which, in spinach PS II, stabilizes binding of Mn but does not provide ligands for Mn (Miller et al., 1987; Cole et al., 1987b), and (3) differences in the gene sequences of D1 and D2 from eukaryotes and prokaryotes (Williams & Chisholm, 1987; Curtis & Haselkorn, 1984; Mulligan et al., 1984). In addition to these differences in the proteins, different biochemical methods are generally used in preparing PS II from prokaryotic organisms and plant chloroplasts. A multiline EPR signal similar to that observed in the S_2 state in spinach has also been observed in cyanobacteria (Ke et al., 1982) indicating that at least part of the Mn complex is similar in the two classes of organisms. However, a detailed comparison of the spectral properties of the Mn complex in PS II between cyanobacteria and plants is lacking. Our objectives in this study are to (1) develop and characterize a preparation of PS II from a thermophilic cyanobacterium, *Synechococcus* sp., with active O_2-evolving PS II reaction centers and a homogeneous Mn content, (2) characterize the S_1 to S_2 advance so that S_1 and S_2 state samples may be prepared, and (3) characterize the structure and oxidation states of the Mn cluster from *Synechococcus* in the S_1 (dark adapted) and S_2 states by EPR and X-ray absorption spectroscopy. The comparison of PS II prepared from *Synechococcus* and spinach yields a larger perspective on the salient and essential features of the Mn complex.

Materials and Methods

Preparation of PS II. This photosystem II preparation is similar to one recently reported from *Synechococcus* (Satoh et al., 1985). Thermophilic *Synechococcus* sp., a generous gift of Prof. S. Katoh, University of Tokyo, was grown at 50–55 °C in 50–100 L of a medium similar to that described previously (Dyer & Gafford, 1961) with increased copper and iron concentrations of 75 μM each (as $CuSO_4$ and $FeCl_3$). Whole cells were collected with a continuous-flow Sharples centrifuge. The cells were washed in 50 mM HEPES, pH 7.5, 10 mM NaCl, and 1 mM PMSF and centrifuged at 16000*g* for 12 min. The cells were then incubated with 100 mg of lysozyme at 37 °C for 1 h in the dark in 100 mL of a medium containing 0.4 M mannitol, 5 mM EDTA, 50 mM HEPES, pH 7.5, and 1 mM PMSF. The cells were then centrifuged as above and resuspended in a medium containing 50 mM MES, pH 6.2, 10 mM NaCl, and 1 mM PMSF. This suspension was passed twice through a French pressure cell operating at 435 atm to obtain thylakoid fragments. The DNA in the resulting suspension was degraded by addition of approximately 1 μg of DNase (Sigma) and 5 mM $MgCl_2$. This mixture was stirred at 0 °C for 1 h in the dark. The DNase reaction was stopped by addition of EDTA to make 10 mM. Unbroken cells were removed by centrifugation at 12000*g* for 15 min, and thylakoid fragments were collected by centrifuging at 300000*g* in a Ti50.2 rotor (Beckman) for 1 h. The thylakoid fragments were resuspended in a medium containing 0.5 M sucrose, 50 mM MES, pH 6.2, 10 mM NaCl, 5 mM $MgCl_2$, and 0.5 mM PMSF (medium A). The suspension was then spun at 12000*g* for 10 min, and the thylakoid fragments were collected by centrifugation as described above.

The thylakoid fragments were resuspended in medium A to a concentration of 1 mg of Chl mL^{-1}, and the PS II was extracted at 21–22 °C under dim light with the detergent octyl β-glucoside. During each preparation a range of detergent concentrations from 0.4 to 0.8% was tested in small aliquots of sample. The test samples, which had a clearing distance of 0.8 cm, were then spun at 300000*g* for 30 min. The supernatants of this spin were analyzed for Chl, P700, and O_2 evolution activity (as described below). The optimum detergent concentration to extract over 85% of the O_2 evolution activity with less than 2% of the P700 of the unfractionated thylakoid fragments was approximately 0.63%. This extract also contained approximately 10–15% of the total chlorophyll. The bulk of the thylakoids was then extracted with the optimum detergent concentration. The thylakoid detergent mixture was then centrifuged at 300000*g* for 2.5 h, with a clearing distance of 12 cm. The supernatant of this spin was collected and diluted with an equal volume of water, and the PS II was concentrated by centrifugation at 300000*g* for 3 h. Before the resulting PS II pellet was frozen at 77 K, an equal

volume of glycerol was added to the sample.

We caution that the extraction of PS I occurred at a detergent concentration of approximately 0.8%, *only 0.15% higher than the extraction of PS II.* To avoid contamination by PS I, it is critical that the bulk of the preparation be extracted under the same conditions (especially temperature) as the survey aliquots.

The thylakoid fragments typically had a specific O_2 evolution activity of 300 μmol of O_2 (mg of Chl)$^{-1}$ h^{-1}. PMSF was found to be important for preserving the O_2 evolution activity. Assays of O_2 evolution activity (as described below) directly following cell disruption indicated that the total O_2 activity was stable. The activity was also quite stable in the EDTA treatment step, although we have observed that repeated washes with EDTA may lead to inactivation. To characterize the stability of the oxygen evolution activity during purification of PS II, we use the "total O_2 evolution activity", a quantity defined as the specific activity multiplied by the total Chl. In contrast to activities which are normalized to the amount of Chl, the total O_2 evolution activity does not depend on the amount of Chl present per reaction center. The total O_2-evolution activity was quite stable during the extraction of PS II, and any activity that was missing from the PS II supernatant was found in the pellet. However, we have found that the use of octyl β-glucoside in the presence of higher concentrations of NaCl or other salts causes a slow decline in total activity and a release of Mn. Specific activities of the resulting PS II were approximately 2000 μmol of O_2 (mg of Chl)$^{-1}$ h^{-1} when measured at 21–23 °C.

Chemical and Biochemical Analysis. The preparations were analyzed for Chl by optical absorption measurements following extraction into 80% acetone (Arnon, 1949). Analysis for P700 was done by optical bleaching measurements at 699 nm during illumination with blue actinic light in a medium containing 50 mM Tris, pH 7.5, 10 mM ascorbate, 1 mM methyl viologen, and 0.1 μM PMS. The sensitivity of these assays is such that 1% of the P700 from the thylakoids could easily be detected in the PS II preparation. O_2 evolution assays were measured at 2–20 μM Chl in a suspension medium containing 50 mM MES, pH 6.2, 0.5 M sucrose, 10 mM NaCl, 5 mM $CaCl_2$, 0.5 mM DCBQ, 1 mM $K_3Fe(CN)_6$, and 1 mM K_4-$Fe(CN)_6$ with a Clark-type O_2 electrode biased at −0.6 V vs Ag/AgCl during saturating actinic illumination of the sample. Estimation of the PS II reaction center concentration was made by integrating the EPR signals resulting from D^+ and Z^+ (Babcock et al., 1983). The Mn content was determined (for the same samples) by atomic absorption analysis of nitric acid digested samples.

Illumination and EPR Analysis. PS II samples prepared as described above were dark adapted for 1–2 h and frozen in liquid nitrogen. The samples were illuminated for 2 min with a 400-W tungsten lamp with a heat filter (consisting of a 3-cm path of 5% aqueous $CuSO_4$). During illumination the sample was maintained at a given temperature with N_2 gas flow and monitored with a copper–constantan thermocouple. The EPR spectra were measured on a Varian E-109 spectrometer equipped with a Model E102 microwave bridge and an Air Products Helitran liquid helium cryostat.

EPR signal amplitudes were measured as peak-to-trough amplitudes in the first-derivitive spectrum for the Fe^{2+}–Q signals at g = 1.8 and 1.6. The multiline amplitude was measured similarly, by use of the fourth and fifth hyperfine lines downfield from g = 2. In spectra with the the g = 1.8 and g = 1.6 signals, it is difficult to estimate their amplitudes because they overlap; in these cases the amplitudes were estimated by simulating the spectra with sums of spectra that contain only one signal. The amplitudes were normalized to correct for variable sample concentrations and volume.

X-ray Absorption Measurements. X-ray absorption K-edge spectra were measured on beamline IV-1, and EXAFS spectra were measured on beamlines VI-2 and IV-2 during dedicated operation of the SPEAR storage ring at the Stanford Synchrotron Radiation Laboratory (SSRL). For X-ray absorption edge studies Si⟨111⟩ monochromator crystals were used, and for EXAFS spectra Si⟨400⟩ crystals were used. While the Si⟨111⟩ crystals have an approximately fourfold higher throughput, they were not used for Mn EXAFS studies because in the energy range used for Mn EXAFS they have large "glitches", energies at which a large fraction of the beam is diffracted away. For all comparisons of Mn XAS spectra of PS II from spinach and *Synechococcus*, an identical experimental arrangement was used. The initial X-ray flux was measured with a NE104 plastic scintillator and photomultiplier tube assembly measuring the total photomultiplier current due to X-rays scattered from a thin Mylar film. The sample fluorescence was monitored (Jaklevic et al., 1977) with a NE104 plastic scintillation array for photon counting as described previously (Powers et al., 1981) or with a United Scientific Corp. lithium-drifted silicon solid-state (Si–Li) detector. The X-rays that were scattered from the PS II sample were selectively absorbed by placing a Cr filter between the sample and detector (Stern & Heald, 1979). The EXAFS data in this paper were collected with the Si–Li detector while all of our previously reported Mn EXAFS data of spinach PS II were collected with the photomultiplier tube assembly. In contrast to the photomultiplier tube assembly, the Si–Li detector is capable of energy discrimination. The resolution of the detector during these experiments, approximately 330 eV (fwhm), is sufficient to allow discrimination between various components of the incident flux at the detector. These include the 2p–1s Mn fluorescence, the scattered X-rays, the fluorescence of the Cr filter, and fluorescence or scattering associated with beam harmonics. Using the Si–Li detector, we selectively recorded the Mn fluorescence, thus decreasing the noise and artifacts associated with other components. A more detailed description of the detectors is available (McDermott, 1987). Energy calibration was maintained by simultaneously measuring the absorption spectrum of $KMnO_4$ with two additional detectors (Goodin et al., 1979).

During X-ray absorption measurements the samples were routinely maintained below −90 °C with a liquid nitrogen boil-off jet. For the 140 K illuminated samples, X-ray measurements were made between 150 and 160 K. The samples were prepared in a lucite sample holder in which illumination, EPR, and X-ray absorption measurements could be made. The EPR spectra of the samples were measured both before and after X-ray beam exposure to ensure sample integrity.

Data Analysis. The general data analysis procedures have been described in a recent article (Yachandra et al., 1986). Specific procedures are detailed in the figure captions or under Results.

Results

Characterization of the Preparation. This preparation of PS II from *Synechococcus* results in an improvement in the PS II to PS I ratio of approximately 50 and in a yield of greater than 80% of O_2 evolution activity relative to unfractionated thylakoid fragments. The stability of the steady-state O_2 evolution activity is excellent under the conditions of the preparation procedure and during data collection. Analysis of the preparation indicates 3.5 ± 0.5 Mn and 60–70 Chl per

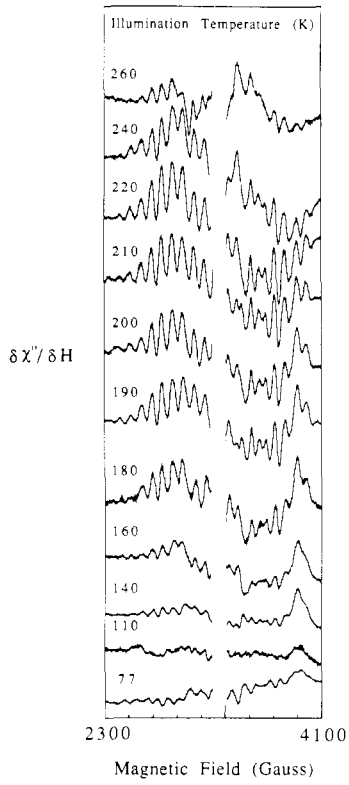

FIGURE 1: Illuminated minus dark EPR spectra of PS II from *Synechococcus* taken at 8 K following continuous illumination for 1.5 min at the indicated temperature. A section of the spectrum near $g = 2$ has been removed. Spectrometer conditions were 9.21 GHz, 50 mW, 32 G at 100-kHz field modulation, and a gain of 5000. The observation temperature (8 K) and microwave power were chosen for optimal observation of the multiline signal. The broad multiline signal centered at $g = 2$ strongly resembles the multiline signal observed in spinach PS II particles in the S_2 state. The maximum amplitude of the multiline signal is seen in samples illuminated at 220 ± 10 K.

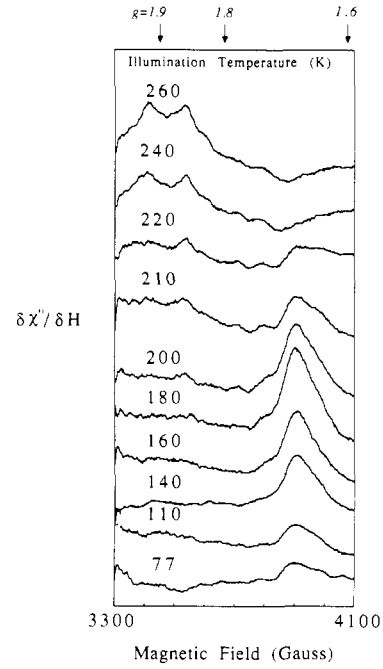

FIGURE 2: Illuminated minus dark EPR spectra of PS II from *Synechococcus* taken at 5 K following continuous illumination at the indicated temperature for 1.5 min. The observation temperature (5 K) was chosen for optimal observation of the Fe^{2+}–Q_A^- signal with minimal interference from the multiline signal. The signals at $g = 1.8$ and 1.9 generated at 240 and 260 K are due to Fe^{2+}–Q_A^- and Fe^{2+}–Q_B^-; at 180 K and below, the signal due to Fe^{2+}–Q_A^- appears at $g = 1.6$ instead. The smaller amplitude of the signal generated by illumination at 110 and 140 K, as compared with the signal generated by illumination at 180 K, is due to nonsaturating illumination at lower temperatures. The spectra collected after illumination at 200, 210, and 220 K reflect the $g = 1.6$ signal together with the $g = 1.8$ and 1.9 signals. Other spectrometer conditions are as in Figure 1.

reaction center. Despite the fact that the preparation is largely stripped of its light harvesting system and resembles core preparations in peptide content, the concentration of Mn in a dense pellet is not higher than that in spinach Triton X-100 preparations (Yachandra et al., 1986); both are approximately 700 μM in Mn. Our cursory evaluation of a recent O_2-evolving core preparation from spinach (Ghanotakis & Yocum, 1986) indicates that it also does not allow a significant improvement in reaction center concentration (or Mn concentration) in a dense pellet.

EPR Studies of the S_1 to S_2 Transition at 220 K. Figure 1 shows the multiline signal generated during continuous illumination at several different temperatures. The maximal amplitude is developed at approximately 220 K. Three observations suggest that the conversion from S_1 to S_2 in active centers is essentially complete when conducted at 220 K (data not shown): (1) the multiline signal amplitude is linear with concentration of PS II, (2) the multiline amplitude reaches a maximum with respect to illumination time by 15 s and remains constant with longer illumination, and (3) the same amplitude of the multiline signal is generated by continuous illumination at 215 K as by illumination at ice temperature in the presence of DCMU, which leads to single turnover photochemistry (Joliot, 1974). Our sample preparation protocols involve resuspending the PS II in a buffer containing 50% glycerol for illumination and EPR measurements. In our experience, the glycerol is necessary to observe the multiline EPR signal.

The $g = 1.8$ and $g = 1.9$ acceptor signals which form upon illumination at 240 K, shown in Figure 2, are similar to the signals formed in spinach PS II (Rutherford & Zimmermann, 1984). The spectra in Figure 2 were measured at 5 K; at this temperature the multiline signal saturates at lower microwave power than do the iron–semiquinone signals, and spectra taken at 50 mW reflect mainly the iron–semiquinone species with little contribution from the multiline spectrum. Although there are two separate signals at $g = 1.9$ and $g = 1.8$, within our signal-to-noise ratio both signals vary in a similar fashion with illumination temperature. In estimating the amplitudes of these signals, we do not distinguish between them and we refer to the composite as "the 1.8 signal".

EPR Studies of the S_1 to S_2 Transition at 140 K. Figure 1 shows that when the illumination is conducted at temperatures below 190 K the amplitude of the multiline EPR signal produced is smaller. In PS II preparations from spinach, the loss of the multiline signal amplitude at lower illumination temperatures is paralleled by the growth of an EPR signal at $g = 4.1$ (Casey & Sauer, 1984; de Paula et al., 1985) which has been assigned to Mn in the S_2 state (Zimmermann & Rutherford, 1986; Cole et al., 1987a). In our preparations, no light-induced signal at $g = 4.1$ is seen. We have extensively and unsuccessfully searched for a Mn signal or other donor species signal from the samples illuminated at 140 K, using microwave powers ranging from 10 μW to 50 mW, measurement temperatures from 4.3 to 25 K, and field values ranging from $g = 8$ to $g = 1.5$. In particular we do not see a substantial light-induced $g = 2$ radical signal or a light-induced cyt *b*-559 signal. In addition, warming the 140 K illuminated sample to 215 K for 2 min does not result in a donor signal.

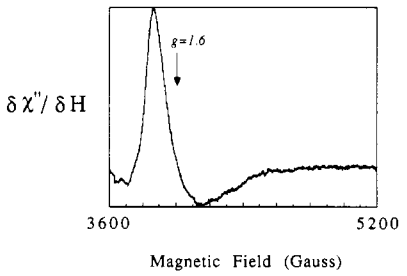

FIGURE 3: Illuminated minus dark EPR spectra at 5 K of PS II from *Synechococcus* following continuous illumination at 140 K for 2 min illustrating the line shape of the $g = 1.6$ EPR signal. Spectrometer conditions are as in Figure 2.

Figure 2 shows that at lower illumination temperatures the $g = 1.9$ and $g = 1.8$ signals assigned to Fe^{2+}–Q_A^- are absent. Upon illumination in the range of 110–180 K, we observe a previously unreported signal near $g = 1.6$ (Figure 2). Figure 3 illustrates the first-derivative line shape of this signal, which has a broad absorption; the separation between the first-derivative maximum and minimum is 300 ± 50 G. The rising edge of this signal is relatively sharper than the falling edge, and its maximum (i.e., the zero crossing of the first derivative) corresponds to a g value of 1.64 ± 0.03. Measurements at 9.19 and 8.87 GHz indicate a change in the first-derivative maximum from 3920 to 3780 G, confirming that the resonance field position reflects the g value of the signal and not zero field splittings (McDermott, 1987). This signal is not saturated at microwave powers up to 100 mW at 5 K, indicating a very rapid spin relaxation pathway, and the temperature dependence of the amplitude between 5 and 20 K is consistent with a ground-state species.

The dependence of the EPR signal amplitudes on temperature of illumination is shown in Figure 4. The amplitude of the $g = 1.6$ signal is complementary to that of the $g = 1.8$ signal, suggesting that it is an acceptor species (Figure 4a). A likely assignment is an alternative configuration of the Fe^{2+}–Q complex. The sensitivity of this signal to various chemical treatments supports this assignment (McDermott, 1987). Treatment with 25 mM sodium formate at pH 6.0 followed by dark adaptation and illumination at 140 K does not produce the $g = 1.6$ signal, but a signal at $g = 1.8$ appears, with a first-derivative line shape similar to an Fe^{2+}–Q_A^- signal seen in formate-treated spinach PS II (Vermaas & Rutherford, 1984). Treatment with DCMU inhibits O_2 evolution in the preparation from *Synechococcus*. Illumination of DCMU-treated PS II preparations at 140 K does not result in formation of the signal at $g = 1.6$ but results in signals at $g = 1.8$ and 1.9. Two treatments that remove Mn and extrinsic PS II proteins, incubation in 0.8 M Tris at pH 8.5 or treatment with 0.5 mM NH_2OH, cause a decreased amplitude of the $g = 1.6$ signal induced by 140 K illumination to 30% of the control amplitude.

X-ray Absorption K-Edge Studies of Manganese. Figure 5 compares the Mn X-ray absorption K-edge spectra of PS II prepared in the S_1 state and in the S_2 state by 215 K illumination. Upon illumination the edge inflection shifts by 0.8 ± 0.2 eV from approximately 6550 to 6551 eV, indicating an oxidation of Mn. In the K-edge spectra of Mn in the S_1 and the S_2 states, smaller amplitude transitions at 6541 eV ("preedge features") are apparent. The spectrum of the S_2 sample has a trough between the preedge feature and the main edge transition in which the absorbance is less than half that of the maximum of the preedge feature (Figure 5b). In contrast, the spectrum of the S_1 sample has only a small decrease in absorbance between the preedge maximum and the main edge transition. Thus, the S_1 to S_2 transition is accompanied by not only a shift in Mn K-edge inflection energy but also a change in Mn K-edge structure. The shape of the preedge features is very similar in the Mn K-edge spectra of PS II from *Synechococcus* and spinach. Furthermore, the change in preedge structure from the S_1 to the S_2 state is seen in preparations from both organisms. For both S_1 and S_2 samples, the Mn K-edge inflection energy is 0.5 ± 0.3 eV lower for Mn in PS II from *Synechococcus* as compared to that for Mn in PS II from spinach (Yachandra et al., 1987).

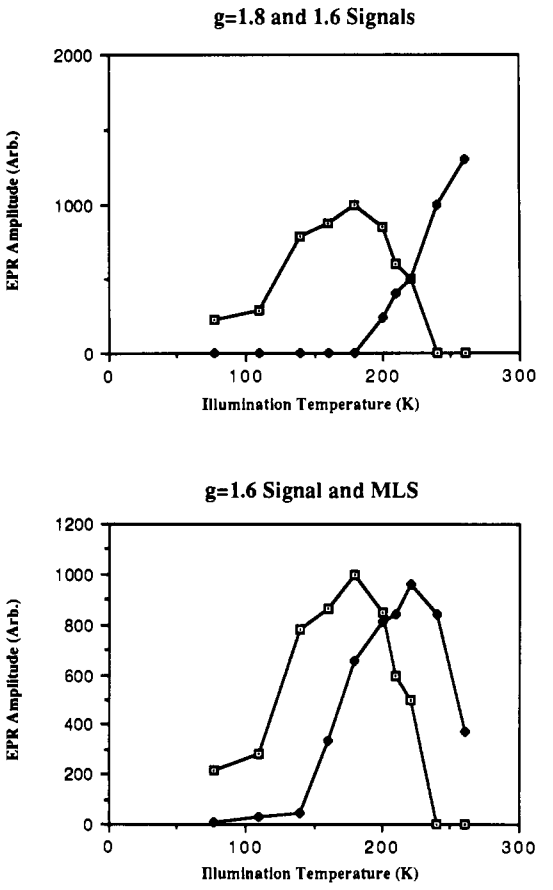

FIGURE 4: Signal amplitudes for EPR signals generated by illumination of *Synechococcus* PS II particles are plotted as a function of the illumination temperature. In the top panel, solid dots refer to the $g = 1.8$ and 1.9 signals, and in the bottom panel, they refer to the multiline signal. In both panels the open dots refer to the $g = 1.6$ signal. In the spectra of samples illuminated at 200, 210, and 220 K the $g = 1.8$ and $g = 1.6$ signals overlap and cancel. Therefore, their amplitudes were estimated by simulations using sums of the 240 and 180 K spectra. The amplitude of the multiline signal was measured by use of the fourth and fifth hyperfine lines downfield from $g = 2$. (a) shows that the amplitude of the $g = 1.6$ signal is complementary to that of the $g = 1.8$ signal between 180 and 240 K, while (b) shows that the amplitude of the multiline signal is not complementary to that of the $g = 1.6$ signal.

Figure 6 compares the Mn K-edge spectra of S_2 states prepared by illumination at 215 K and by illumination at 140 K. A similar edge position is seen in the two samples, indicating that Mn was oxidized upon illumination at 140 K. The preedge region in the spectrum of the 140 K illuminated sample exhibits a trough between the preedge maximum and the main edge transitions as does the spectrum of the sample illuminated at 215 K, while the amplitude of the preedge feature is higher in the spectrum of the 140 K illuminated sample.

X-ray Absorption Fine Structure Studies of Manganese. Figure 7 shows Fourier transforms of the Mn EXAFS data of the 215 K illuminated S_2 state of PS II from *Synechococcus*.

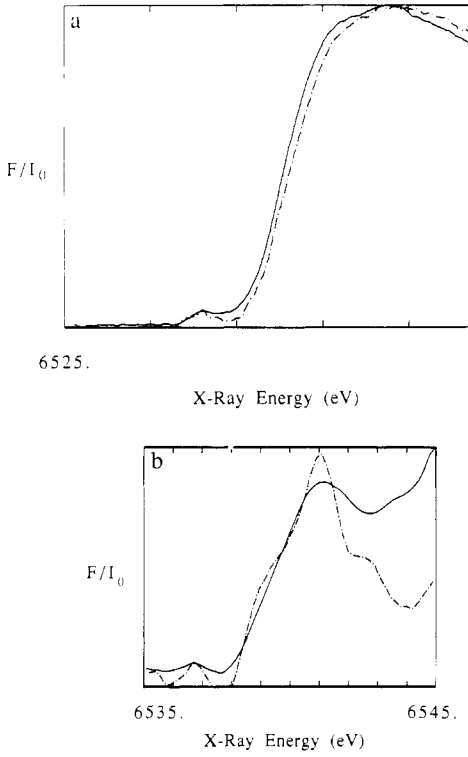

FIGURE 5: Mn K-edge X-ray absorption spectra of *Synechococcus* PS II particles prepared in the S_1 state by dark adaptation (solid line) and the in S_2 state by continuous illumination at 215 K following dark adaptation (dashed line). The data were smoothed with a domain of approximately 1 eV. The edge inflection energy of the S_2 sample is 0.7 eV higher than that of the S_1 sample (a). The features at approximately 6541 eV (just before the edge) are due to semiforbidden 1s–3d transitions and are expanded in (b). These features resemble respectively those of Mn(III) complexes in the S_1 state and those of Mn(IV) complexes in the S_2 state (Sauer et al., 1988).

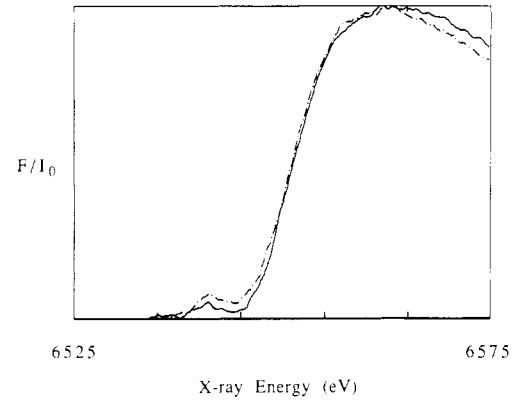

FIGURE 6: Mn K-edge X-ray absorption spectra of *Synechococcus* PS II particles prepared in the S_2 state by dark adaptation followed by continuous illumination at 215 K (solid line) and at 140 K (dashed line). The data were smoothed with a domain of approximately 1 eV. The two edge inflection energies are indistinguishable from each other, indicating that the oxidation states are the same, and both are oxidized relative to S_1. The structure of the preedge for the 140 K illuminated sample also resembles those of Mn(IV) complexes, but has a higher intensity than that of the 215 K illuminated sample.

The k-space data are multiplied by k^1 or k^3 to emphasize first row ligands or transition metal neighbors, respectively. The Fourier transforms have two main features: a peak at $R + \Delta = 1.2$ Å which is due to O or N (peak I) and a peak at approximately $R + \Delta = 2.2$ Å which is principally due to a transition metal (peak II). The third peak at $R + \Delta = 3$ Å is barely above the noise level and is somewhat variable; we have been unable to determine whether this peak is due to a

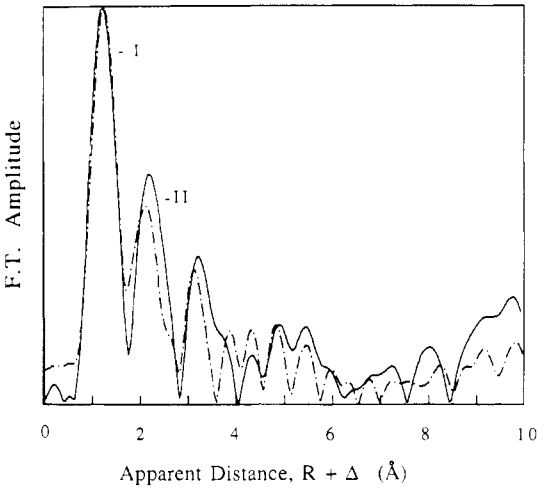

FIGURE 7: Fourier transforms of the k^1 (dashed line) and k^3 (solid line) weighted Mn EXAFS data of *Synechococcus* in the S_2 state (using data of range $k = 3.4$–10.9 Å^{-1}). The first peak is primarily due to bridging O (or N) ligands at 1.75 Å and terminal ligands. The second peak is primarily due to transition metal neighbor(s) at 2.7 Å. These peaks are characteristic of a di-μ-oxo-bridged Mn cluster. The peaks appear at an apparent distance which is shorter than the internuclear distance by an amount Δ which may be approximated by $(1/2)\langle\delta\alpha/\delta k\rangle$.

transition metal or a first row element(s) or both.

Figure 8 shows simulations by the Teo–Lee method (Teo & Lee, 1979) of k^2-weighted Fourier filtered data. The filtered data include EXAFS data from $k = 3.5$ to $k = 11$ Å^{-1}, Fourier filtered to include features from $R + \Delta = 0.5$–2.8 Å (to include both shells) or from $R + \Delta = 1.7$–2.8 Å (to include the second shell only). The data along with the two-shell Fourier filtered data are also shown in Figure 8f. An extensive search for acceptable simulations of these data indicates that it is essential to include a first row transition metal neighbor at 2.7 Å and C, N, or O at 1.75 Å. The transition metal neighbor at $R + \Delta = 2.2$ Å is very likely to be another Mn atom, since simulations of the multiline EPR spectrum indicate that at least two Mn are required to explain the hyperfine structure (Dismukes & Siderer, 1981; Dismukes et al., 1982; Hansson & Andréasson, 1982). On the basis of chemical precedent, we assume that the bridging atom(s) is (are) oxygen.

Simulations of peak II indicate that a symmetric tetranuclear structure is unlikely (Figure 8). The best simulations involved one Mn neighbor at 2.7 Å, together with O, C, or N neighbors at approximately 3.2 Å, which are presumeably second-shell ligand atoms (Figure 8c, Table I). Simulation of the Mn peak assuming three Mn neighbors did not adequately reproduce the amplitude or the shape of the envelope (Figure 8b) *regardless of what value for the Debye–Waller factor was used.*

Simulations of peaks I and II together lead to the same conclusion. Figure 8c shows a best fit to the data for three types of neighboring atoms which had parameters corresponding very closely to binuclear structures, including one to two μ-oxo ligands at 1.75 Å, three to four additional O neighbors in a range of distances between 1.9 and 2.3 Å, and 1–1.5 Mn neighbor(s) at 2.75 Å. The distances and number of scatterers obtained for the first-shell ligands in these simulations are within error of those obtained by fitting the first shell alone. The S_1 data (not shown) can be simulated by very similar parameters. For comparison, two less satisfactory simulations of peaks I and II of the S_2 data are shown in panels d and e of Figure 8. In these simulations each Mn is assumed to have three Mn neighbors, three μ-oxo ligands, and one (Figure 8d) or three (Figure 8e) terminal ligands to mimic

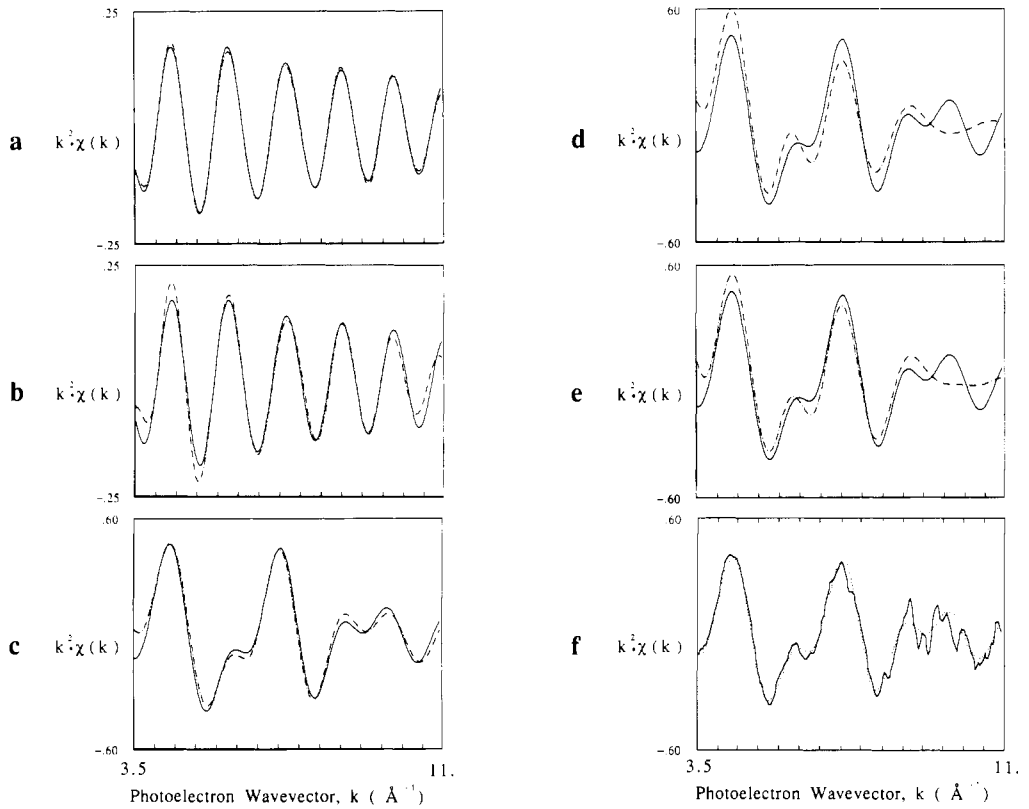

FIGURE 8: Simulations of Fourier filtered Mn EXAFS data of PS II from *Synechococcus*, weighted by k^2, including only peak II (a and b) or peaks I and II (c–e). The Fourier filtered data (solid line) are shown with the best simulation with no assumptions about numbers of neighboring atoms (dotted line, a and c) or with an optimized simulation using numbers of neighbors characteristic of tetranuclear clusters (dotted line, b, d, and e). The Debye–Waller parameters were optimized for quality of fit in each case. (d) is a simulation of a relatively symmetric adamantane-like tetranuclear cluster which would involve four-coordinate Mn, while (e) is a simulation of a cubelike tetramer which would involve six-coordinate Mn. The simulations indicate that both of these structures are unlikely. The best simulations (a and c) had numbers of ligands similar to those of dimeric clusters. However, these data may also be consistent with a highly distorted tetrameric cluster in which the backscattering due to various Mn neighbors interferes. The parameters of the simulations are listed in Table I. In (f) the raw EXAFS data (smoothed by calculating running average over a range of 0.1 Å^{-1}) are shown for comparison with the Fourier filtered data (f). (Details of the Fourier filtering are shown under Results.)

Table I: EXAFS Simulation Parameters[a]

figure	neighboring atom	R (Å)[b]	N[c]	σ (Å)[d]	fit error[e]
Figure 8a (best fit of peak II)	Mn	2.76	1.3	0.10	0.006
	O	3.27	2.0	0.10	
Figure 8b (three-Mn fit of peak II)	Mn	2.75	3.0	0.10	0.08
	O	3.23	1.4	0.01	
Figure 8c (best fit of peaks I and II)	O	1.74	1.6	0.08	0.10
	O	2.21	3.4	0.22	
	Mn	2.69	1.3	0.13	
Figure 8d (adamantane fit of peaks I and II)	O	1.78	3.0	0.18	1.40
	O	2.18	1.0	0.09	
	Mn	2.70	3.0	0.22	
Figure 8e (cube fit of peaks I and II)	O	1.80	3.0	0.16	0.76
	O	2.18	3.0	0.16	
	Mn	2.68	3.0	0.19	

[a] Simulations were done by the method of Teo and Lee (1979) and are shown in Figure 8. In addition to the parameters listed, in these simulations we vary the E_0 value for each shell separately. The range for ΔE_0 was restricted to −10 to 10 eV where E_0 was 6550 eV. [b] R is the internuclear distance between the absorbing Mn and the neighbor. Typical uncertainties are 0.03 Å. [c] N is the number of neighboring atoms, which is adjusted from the value determined in the simulation by a factor of 2 as described (Teo & Lee, 1979). Typical uncertainties are 25%. [d] σ is the Debye–Waller parameter, equal to the rms sum of static and dynamic disorder in the internuclear distance, R. Typical errors are 0.02 Å. [e] The fit error is a relative measure of the sum of absolute values of the residuals of the simulation, at the indicated k weighting.

four-coordinate and six-coordinate symmetric tetranuclear clusters. Again, regardless of the Debye–Waller factor used in the "symmetric tetramer" simulations, we cannot obtain better agreement for a symmetric tetranuclear simulation than those shown in panels d and e of Figure 8.

The full set of parameters used in these simulations is presented in Table I.

Discussion

S_1 to S_2 Transition at 220 K. Illumination at 210–240 K results in a charge separation involving Mn as the ultimate electron donor and Q_A as the acceptor, and the oxidized donor gives rise to a multiline EPR spectrum with 88-G splittings, quite similar to that seen in spinach. The acceptor signal includes the g = 1.8 and 1.9 signals previously reported for spinach PS II, together with a new EPR signal at g = 1.6. Illumination at temperatures above 240 K leads to a smaller amplitude of the multiline signal when no DCMU is included. These data demonstrate that the temperature at which a maximal multiline signal is formed is higher for *Synechococcus* (220 K) than for spinach (190 K), possibly because in *Synechococcus* S-state conversion rates or Q_A to Q_B electron-transfer rates are different from those in spinach.

A New EPR Signal at g = 1.6. After illumination at 110–160 K, the multiline EPR spectrum of the Mn donor and the g = 1.8 and 1.9 EPR spectra of the Q_A acceptor are absent, but a new signal at g = 1.6 appears. Presumably this signal is due to an oxidized donor or a reduced acceptor. The amplitude of the g = 1.6 signal is complementary to the amplitude of the g = 1.8 and 1.9 signals in the temperature range from 180 to 240 K (Figure 4a). In the same range of illumination temperatures the multiline signal amplitude varies by less than

20% from the maximal value and is not complementary to the amplitude of the $g = 1.6$ signal (Figure 4b). These observations are suggestive that the $g = 1.6$ signal and the $g = 1.8$ signal are both acceptor signals. Electron transfer from the reaction center primary pigment to Q_A proceeds at temperatures as low as 5 K in spinach PS II preparations and in purple nonsulfur bacteria (Nugent et al., 1981; Butler et al., 1984). Q_A to Q_B electron transfer is blocked below 190 K in spinach (de Paula et al., 1985) and probably below 220 K in *Synechococcus*. Therefore, it is very likely that Q_A is the acceptor in this preparation at 140 K and that the $g = 1.6$ signal is associated with Q_A.

Two treatments that are thought to affect the acceptor complex specifically have a dramatic effect on the $g = 1.6$ signal. Addition of formate followed by illumination at 140 K results in a signal with a g value and line shape like those of the altered Fe^{2+}–Q_A^- signal seen in formate-treated spinach PS II particles (Vermaas & Rutherford, 1984), while the $g = 1.6$ signal is no longer present. Formate is thought to bind in the acceptor complex at the same site as bicarbonate. A recent review of the mechanism of the formate effect is available (Govindjee & Eaton-Rye, 1986). The conversion of the $g = 1.6$ signal to a $g = 1.8$ signal on formate addition indicates that the acceptor species at 140 K is Q_A and that it gives rise to the $g = 1.6$ signal. Further, the $g = 1.6$ signal is affected by binding of DCMU at the Q_B site, while the donor side is not affected, as evidenced by the presence of the multiline signal. In this respect it is noteworthy that binding of quinones and quinone analogues at the Q_B site alters the Fe^{2+}–Q_A^- signals in cyanobacteria and higher plants (Atkinson & Evans, 1983; Rutherford et al., 1984).

In contrast, treatments that are specific to the donor complex have relatively less effect on the $g = 1.6$ signal. Following treatments with hydroxylamine or Tris, 30% of the $g = 1.6$ signal appeared despite abolition of O_2 evolution activity. The decreased amplitude of the $g = 1.6$ signal on release of Mn by Tris or hydroxylamine treatment is suggestive that the efficiency of stable electron transfer decreases in the absence of a competent donor.

These data indicate that the Fe^{2+}–Q_A^- species exhibits two different EPR signals depending on the temperature of illumination. It is possible that the $g = 1.6$ form is a conformationally excited form of the Fe^{2+}–Q_A^- complex that cannot relax at lower temperatures. Upon incubation with formate, only one form of the Fe^{2+}–Q_A^- signal is seen in *Synechococcus*; it resembles the Fe^{2+}–Q_A^- signal seen in spinach PS II following formate treatment. Formate may bind at the iron in a site analogous to the glutamate (M232) ligand in bacterial reaction centers (Deisenhofer et al., 1985). We speculate that the conversion from the $g = 1.6$ to the $g = 1.8$ form of the Fe^{2+}–Q_A^- complex could involve changes in the iron carboxy ligand and that the existence of the $g = 1.6$ signal in *Synechococcus* but not plants could signify differences in the iron carboxy ligation for the two organisms. There are many differences between the region of the glutamate ligand in the M subunit and the analogous region of D2, (Hearst, 1986); this region of D2 also differs between cyanobacteria and plants (Williams & Chisholm, 1987).

The signal from Fe^{2+}–Q_A^- in purple nonsulfur bacteria at $g = 1.8$ has been modeled in terms of the $S = 2$ states of the Fe^{2+} system coupled to the $S = {}^1/_2$ semiquinone radical (Butler et al., 1980, 1984; Dismukes et al., 1984); this treatment may be useful for describing the $g = 1.6$ signal as well. A second-order perturbation treatment describing the exchange interaction between the semiquinone and the iron yields an expression for the resulting g value: $g = g_Q[1 - 2(J/\Delta E_{1,2})^2]$, where g is the observed g value of the coupled iron–semiquinone system, J is the exchange coupling between the semiquinone and the iron, g_Q is the g value of an isolated semiquinone, and $\Delta E_{1,2}$ is the splitting between the two lowest M_S states in the $S = 2$ manifold of the Fe^{2+} (Butler et al., 1984). If the $g = 1.6$ signal is due to Fe^{2+}–Q_A^-, the g value of 1.6 may result from a large decrease in $\Delta E_{1,2}$ or a large increase in J as compared with the $g = 1.8$ signal. The line shape of the $g = 1.6$ signal shows a relatively steep low-field rising edge and a shallower high-field falling edge as compared with that of the $g = 1.8$ signal. On the basis of higher order perturbation terms, Butler et al. (1984) discuss the effects of J and $\Delta E_{1,2}$ on signal line shapes as well as g values. Their results indicate that changing the zero field splitting parameters is not likely to explain the line shape of the $g = 1.6$ signal but increasing J_z relative to that of the $g = 1.8$ form may explain the line shape and g value.

Illumination at 140 K Results in Mn Oxidation but No MLS or g = 4.1 EPR Signal. At 140 K an apparent acceptor signal is seen, but we are unable to observe a donor signal. The absence of a $g = 4.1$ signal following illumination at 140 K raises the question as to whether Mn is oxidized upon illumination at 140 K. To address this point we monitored the Mn K-edge changes upon illumination at 140 K. Our edge study confirms that Mn is the donor at 140 K but that it is EPR silent under the conditions of our experiment. Mn(IV) and Cr(III), which are both d^3 ions, show EPR signals from the $S = {}^3/_2$ ground state with g values near $g = 4$ if they have large zero-field splittings. A monomeric Mn(IV) species has been proposed as an assignment for the light-induced $g = 4.1$ S_2 signal (Hansson et al., 1987). A study of Cr(III) EPR signals (Singer, 1955) indicates that, depending on the relative energies of the microwave quantum and the zero field splitting (between the $M_S = \pm{}^3/_2$ and the $M_S = \pm{}^1/_2$ Kramers pairs), the line shape can vary from (1) a somewhat broad $g = 4$ signal for large zero field splitting, to (2) a broad unresolved signal from zero field to beyond $g = 2$ when the zero field splitting is comparable to the microwave quantum, to (3) a rather sharp $g = 2$ signal for octahedral complexes with negligible zero-field splitting. A similar situation occurs for Mn(IV); examples of $g = 4$ signals (Lynch et al., 1984; Magers et al., 1980) and $g = 2$ signals (Geschwind et al., 1962) are well-known. Some examples of Mn(IV) monomeric species have been reported that may correspond to case 2 described above, in that they possess approximate octahedral symmetry and show very broad EPR signals (Hartman et al., 1984; Kessissoglou et al., 1986, 1987). If the $g = 4$ signal in spinach is due to a Mn(IV) species with a large zero-field splitting, our Mn K-edge and EPR data may be explained by proposing that a similar oxidation occurs at 140 K in the *Synechococcus* preparation, but the zero-field splitting is smaller and the EPR signal is too broad to be observed. This EPR-silent state also does not give rise to a multiline signal upon warming, indicating that associated with the structural difference in the Mn site are differences in conformational or electron-transfer dynamics.

The apparent differences in Mn structure between the two organisms may reflect changes in PS II proteins due to the large evolutionary gap between cyanobacteria and plants, or they may reflect differences in the preparation procedure. The most striking evolutionary change is that the *Synechococcus* complex lacks the 18- and 24-kDa proteins found in spinach PS II. These peptides can be removed from spinach PS II by washing with high concentrations of NaCl (Ghanotakis &

Yocum, 1985). The basic structure of the Mn complex is similar in the absence of the 18- and 24-kDa proteins (Cole et al., 1987b; Miller et al., 1987). In contrast to control preparations from spinach or these preparations from *Synechococcus*, illumination of the salt-washed preparations at 140 K resulted in a $g = 2$ donor species (de Paula et al., 1986), possibly because the salt-washing procedure causes an irreversible decreased rate of electron transfer from the Mn complex (Dekker et al., 1984; Cole et al., 1986; Cole & Sauer, 1987). Thus it is difficult to compare the results from these salt-washed preparations to our results from *Synechococcus*.

X-ray Absorption K-Edge Structure Indicates Mn Valences. The Mn X-ray absorption K-edge position and the structure of the K-edge offer a method of valence identification. The edge inflection energies of 6550–6551 eV for S_1 and 6551–6552 eV for S_2 samples are similar to those of Mn-(III/IV) mixed -valence complexes, Mn(IV) complexes, and some Mn(III) complexes (Kirby et al., 1981; Sauer et al., 1988). The 0.5–1.0-eV change in edge inflection observed on advance from S_1 to S_2 is consistent with a one-electron or a two-electron change per four Mn by comparison with inorganic complexes (Kirby et al., 1981; Guiles, manuscript in preparation). The preedge region, in which semiallowed 1s–3d transitions are present, also yields information about the oxidation state. These transitions are formally unallowed by dipole selection rules and generally become "dipole allowed" by mixing with 4p orbitals. The structure of the preedge region of the Mn K-edge transitions is systematically different in Mn(III) and Mn(IV) complexes, most notably in that for Mn(IV) the preedge transitions are resolved from the main edge transition while for Mn(III) complexes they are not (Sauer et al., 1988). These differences in the edge spectra are presumably related to systematic symmetry differences between Mn(III) and Mn(IV) complexes which give rise to differences in the energies of the d electron levels and/or differences in matrix elements for 1s–3d transitions. The preedge region of the K-edge spectra of S_1 samples resembles those of many Mn(III) complexes, while for S_2 samples this region of the spectrum resembles those of Mn(IV) complexes. These results are strongly suggestive that in the S_1 to S_2 transition a Mn(III) atom(s) is (are) oxidized to Mn(IV).

The K-edge structure is quite similar in spinach and *Synechococcus* preparations. The similarity of the edge structure and of the multiline spectrum are suggestive that the oxidation states of Mn are the same for the two organisms. The lower edge inflection energy for *Synechococcus* as compared with that for spinach may be due to a difference in the Mn ligands in the two organisms and/or a small amount (<10%) of nonspecifically bound Mn(II). We are unable to account for the structure in the Mn K-edge spectra and the edge position in *Synechococcus* by adding K-edge spectra of octahedral Mn(II) to the K-edge from spinach. In addition, our preparations from *Synechococcus* systematically have less Mn per reaction center (3.5 ± 0.5) than our preparations from spinach (4.8 ± 0.5; Cole et al., 1987b), and we have not observed the characteristic six-line Mn(II) signal in our preparations from *Synechococcus*. Therefore, we think it likely that the difference in the K-edge position for the two organisms results from some change in the ligand environment of the Mn, such as a substitution of N for O.

EXAFS Indicates a μ-Oxo-Bridged Binuclear Cluster. The EXAFS results, particularly the 2.7-Å Mn–Mn distance, offer convincing evidence for a di-μ-oxo-bridged structure in *Synechococcus*. This conclusion was also reached in our previous studies of Mn in PS II from spinach (Yachandra et al., 1987). The use of an energy resolving detector in this work allowed us to collect EXAFS data that were relatively free from background artifacts and that can be simulated with excellent agreement. We are able to retrieve more detailed information from the EXAFS data than was previously possible, especially with regard to the O and N ligands and with regard to determination of the number of ligands and the Debye–Waller factors.

We tested the proposal of relatively symmetrical tetranuclear structures with mostly μ-oxo bridges, such as those illustrated in a recent discussion of the chemistry of H_2O oxidation (Brudvig & Crabtree, 1986). Simulations of the Mn peak at 2.7 Å alone (Figure 8a,b) show that each Mn is μ-oxo bridged to approximately one (and not three) Mn neighbor(s). These simulations include a freely adjustable Debye–Waller parameter to account for the possibility that there exist a range of Mn–Mn distances that are not resolved within the 2.7-Å Mn peak.

One may expect differences between symmetrical tetranuclear complexes and binuclear complexes in the distribution of μ-oxo bridging and terminal ligands as well as in the number of Mn neighbors. In binuclear complexes with a Mn–Mn distance of about 2.7 Å, each Mn has two μ-oxo-bridging O atoms which generally have short Mn–O bond lengths (1.7–1.9 Å) and four terminal ligands which generally have longer bond lengths (2.0 Å or greater). For symmetric tetranuclear structures, each Mn would have three bridging ligands. The 2.7-Å Mn–Mn distance and the 1.7–1.8-Å Mn–O distance have implications with respect to the bond angles and therefore the coordination numbers at the Mn center for tetrameric structures. An adamantane-like tetranuclear structure with these bond distances should involve O–Mn–O bond angles of approximately 114°, which is typical of four-coordinate complexes, while a cubelike tetranuclear structure with these bond lengths would require O–Mn–O bond angles of approximately 90°, as found in six-coordinate complexes. This observation led us to simulate an adamantane cluster as a four-coordinate cluster, including *one* terminal ligand (O, N, Cl, or S), three μ-oxo ligands, and three Mn neighbors (Figure 8d). We simulated a cube as a six-coordinate cluster by including *three* terminal ligands, three μ-oxo ligands, and three Mn neighbors (Figure 8e). (We note that among high-valent multinuclear Mn complexes Mn is almost always found to be six-coordinate, making the cubelike structure more likely.) Both the cubelike and the adamantane-like simulations show much poorer agreement than do simulations with fewer Mn neighbors. Our best simulation (Figure 8c) includes 1.5–2 μ-oxo ligands, three to four terminal ligands, and 1–1.5 Mn neighbors. These parameters are consistent with (1) a complex with two binuclear clusters possessing similar Mn–Mn distances, (2) a binuclear cluster with nearby monomeric Mn atoms, (3) trinuclear structures, or (4) distorted tetranuclear clusters in which each Mn atom has approximately one Mn neighbor at 2.7 Å. There may be additional Mn neighbors at longer distances which are not resolved with the current signal-to-noise ratio. However, considering the amplitude of Mn backscattering in the 2.7-Å peak, it is probably not appropriate to picture all four Mn as μ-oxo bridged in a single symmetric cluster. These conclusions about the Mn environment are quite similar to those derived from studying Mn in PS II from spinach (Yachandra et al., 1987).

It has been suggested that a peroxo-bridged structure is an intermediate for either the S_2 or the S_3 state (Renger, 1978). This proposal has been made on the basis that two-electron oxidation of H_2O to form a peroxo compound is thermody-

namically favored over sequential one-electron oxidations. It is unlikely that Mn atoms which are 2.7 Å apart are bridged by peroxo moieties in either S_1 or S_2, since peroxo-bridged structures are characterized by a longer Mn–Mn distance (Mabad et al., 1985). One may propose that at the S_1 or S_2 stage the oxidizing equivalents are still stored on Mn and therefore the peroxo bridge has not yet formed; this is supported by the edge shifts in the S_1 to S_2 transition together with the absence of structural change in the EXAFS spectrum. On the other hand, one may picture peroxo bridges *between* two binuclear clusters or between a cluster and a monomer. If the resulting Mn–Mn distance is characterized by a large Debye–Waller factor, it would be difficult to observe with our current EXAFS analysis.

Because of the high degree of disorder in the terminal ligands, they contribute a small amplitude to the EXAFS spectrum, and it is difficult to assign them. The nature of these ligands may be addressed in other experiments, many of which will be facilitated by the use of a prokaryote.

Conclusions

(1) The S_1 to S_2 transition occurs on continuous illumination of the PS II preparation from the thermophilic cyanobacterium *Synechococcus* sp. at illumination temperatures between 140 and 220 K, probably involving a formal oxidation state change from Mn(III) to Mn(IV) and reduction of Q_A.

(2) The salient structural features of the Mn in the O_2-evolving complex, as evidenced by EXAFS, are similar in the preparations from *Synechococcus* and spinach. They indicate the presence of a di-μ-oxo-bridged structure, with Mn–O bond length of 1.75 ± 0.05 Å and a Mn–Mn distance of 2.71 ± 0.05 Å in the S_1 and S_2 states. The data are not consistent with a symmetric tetranuclear cluster.

(3) Significant differences in the Fe^{2+}–Q_A^- and in the Mn structures between spinach and *Synechococcus* are evident by EPR when the complexes are illuminated at 140 K. We interpret the new signal at $g = 1.6$ in *Synechococcus* to result from the Fe^{2+}–Q_A^- complex in a different conformational form which probably has a larger exchange coupling between the iron and the semiquinone as compared with the species giving rise to the $g = 1.8$ signal, possibly due to differences in the carboxy ligand of the iron. We suggest that the oxidation of Mn but the absence of the $g = 4.1$ signal on illumination at 140 K may be explained by a change (relative to spinach PS II) in the zero-field splitting parameters of a Mn(IV) monomeric species or a Mn cluster resulting in an extremely broadened EPR signal.

Acknowledgments

We thank Dr. Akihiko Yamagishi for invaluable advice concerning the preparation of PS II from *Synechococcus*, Dr. Jean-Luc Zimmermann and Victoria DeRose for reading the manuscript, and Dr. Joseph Jaklevic for consultation and assistance concerning X-ray detection. We also thank Dr. A. W. Rutherford for suggesting the use of formate to characterize the $g = 1.6$ EPR signal.

Registry No. Mn, 7439-96-5.

References

Arnon, D. I. (1949) *Plant Physiol. 24*, 1–15.

Atkinson, Y. E., & Evans, M. C. W. (1983) *FEBS Lett. 159*, 141–144.

Babcock, G. T., Ghanotakis, D. F., Ke, B., & Diner, B. A. (1983) *Biochim. Biophys. Acta 723*, 276–286.

Britt, R. D., Sauer, K., & Klein, M. P. (1987) in *Progress in Photosynthesis Research* (Biggins, J., Ed.) Vol. 1, pp 573–576, Martinus Nijhoff, Dordrecht, The Netherlands.

Brudvig, G. W., & Crabtree, R. H. (1986) *Proc. Natl. Acad. Sci. U.S.A. 83*, 4586–4588.

Butler, W. F., Johnston, D. C., Shore, H. B., Fredkin, D. R., Okamura, M. Y., & Feher, G. (1980) *Biophys. J. 32*, 967–992.

Butler, W. F., Calvo, R., Fredkin, D. R., Isaacson, R. A., Okamura, M. Y., & Feher, G. (1984) *Biophys. J. 45*, 947–973.

Casey, J. L., & Sauer, K. (1984) *Biochim. Biophys. Acta 767*, 21–28.

Cole, J., & Sauer, K. (1987) *Biochim. Biophys. Acta 891*, 40–48.

Cole, J., Boska, M., Blough, N. V., & Sauer, K. (1986) *Biochim. Biophys. Acta 848*, 41–47.

Cole, J., Yachandra, V. K., Guiles, R. D., McDermott, A. E., Britt, R. D., Dexheimer, S. L., Sauer, K., & Klein, M. P. (1987a) *Biochim. Biophys. Acta 890*, 395–398.

Cole, J. L., Yachandra, V. K., McDermott, A. E., Guiles, R. D., Britt, R. D., Dexheimer, S. L., Sauer, K., & Klein, M. P. (1987b) *Biochemistry 26*, 5967–5973.

Cooper, S. R., Dismukes, G. C., Klein, M. P., & Calvin, M. (1978) *J. Am. Chem. Soc. 100*, 7248–7252.

Curtis, S. E., & Haselkorn, R. (1984) *Plant Mol. Biol. 3*, 249–258.

Deisenhofer, J., Epp, O., Miki, K., Huber, R., & Michel, H. (1985) *Nature (London) 318*, 618–624.

Dekker, J. P., Ghanotakis, D. F., Plijter, J. J., Van Gorkom, H. J., & Babcock, G. T. (1984) *Biochim. Biophys. Acta 767*, 515–523.

de Paula, J. C., Innes, J. B., & Brudvig, G. W. (1985) *Biochemistry 24*, 8114–8120.

de Paula, J. C., Li, P. M., Miller, A.-F., Wu, B. W., & Brudvig, G. W. (1986) *Biochemistry 25*, 6487–6494.

Dismukes, G. C., & Siderer, Y. (1980) *FEBS Lett. 121*, 78–80.

Dismukes, G. C., & Siderer, Y. (1981) *Proc. Natl. Acad. Sci. U.S.A. 78*, 274–278.

Dismukes, G. C., Ferris, K., & Watnick, P. (1982) *Photobiochem. Photobiophys. 3*, 243–256.

Dismukes, G. C., Frank, H. A., Friesner, R., & Sauer, K. (1984) *Biochim. Biophys. Acta 764*, 253–271.

Dyer, D. L., & Gafford, R. D. (1961) *Science (Washington, D.C.) 134*, 616–617.

Geschwind, S., Kisliuk, P., Klein, M. P., Remeika, J. P., & Wood, D. L. (1962) *Phys. Rev. 126*, 1684–1686.

Ghanotakis, D. F., & Yocum, C. F. (1985) *Photosynth. Res. 7*, 97–114.

Ghanotakis, D. F., & Yocum, C. F. (1986) *FEBS Lett. 197*, 244–248.

Goodin, D. B., Falk, K.-E., Wydrzynski, T., & Klein, M. P. (1979) *6th Annual Stanford Synchrotron Radiation Laboratory Users Group Meeting*, SSRL Report No. 79/05, 10–11, Stanford University, Stanford, CA.

Govindjee & Eaton-Rye, J. J. (1986) *Photosynth. Res. 10*, 365–379.

Hansson, Ö., & Andrêasson, L.-E. (1982) *Biochim. Biophys. Acta 679*, 261–268.

Hansson, Ö., Aasa, R., & Vänngård, T. (1987) *Biophys. J. 51*, 825–832.

Hartman, J. R., Foxman, B. M., & Cooper, S. R. (1984) *Inorg. Chem. 23*, 1381–1387.

Hearst, J. E. (1986) *Encycl. Plant Physiol., New Ser. 19*, 382–389.

Jaklevic, J., Kirby, J. A., Klein, M. P., Robertson, A. S., Brown, G. S., & Eisenberger, P. (1977) *Solid State Commun. 23*, 679–682.

Joliot, A. (1974) *Biochim. Biophys. Acta 357*, 439–448.

Joliot, P., Barbieri, G., & Chabaud, R. (1969) *Photochem. Photobiol. 10*, 309–329.

Ke, B., Inoue, H., Babcock, G. T., Fang, Z.-X., & Dolan, E. (1982) *Biochim. Biophys. Acta 682*, 297–306.

Kessissoglou, D. P., Butler, W. M., & Pecoraro, V. L. (1986) *J. Chem. Soc., Chem. Commun.*, 1253–1255.

Kessissoglou, D. P., Li, X., Butler, W. M., & Pecoraro, V. L. (1987) *Inorg. Chem. 26*, 2487–2492.

Kirby, J. A., Goodin, D. B., Wydrzynski, T., Robertson, A. S., & Klein, M. P. (1981) *J. Am. Chem. Soc. 103*, 5537–5542.

Koike, H., & Inoue, Y. (1985) *Biochim. Biophys. Acta 807*, 64–73.

Kok, B., Forbush, B., & McGloin, M. (1970) *Photochem. Photobiol. 11*, 457–475.

Lynch, M. W., Hendrickson, D. N., Fitzgerald, B. J., & Pierpont, C. G. (1984) *J. Am. Chem. Soc. 106*, 2041–2049.

Mabad, B., Tuchagues, J.-P., Hwang, Y. T., & Hendrickson, D. N. (1985) *J. Am. Chem. Soc. 107*, 2801–2802.

Magers, K. D., Smith, C. G., & Sawyer, D. T. (1980) *Inorg. Chem. 19*, 492–496.

McDermott, A. E. (1987) Ph.D. Dissertation, University of California, Berkeley.

Metz, J. G., Pakrasi, H. B., Seibert, M., & Arntzen, C. J. (1986) *FEBS Lett. 205*, 269–274.

Miller, A.-F., de Paula, J. C., & Brudvig, G. W. (1987) *Photosynth. Res. 12*, 205–218.

Mulligan, B., Schultes, N., Chen, L., & Bogorad, L. (1984) *Proc. Natl. Acad. Sci. U.S.A. 81*, 2693–2697.

Nanba, O., & Satoh, K. (1987) *Proc. Natl. Acad. Sci. U.S.A. 84*, 109–112.

Nugent, J. H. A., Diner, B. A., & Evans, M. C. W. (1981) *FEBS Lett. 124*, 241–244.

Pfister, K., Steinback, K. E., Gardner, G., & Arntzen, C. J. (1981) *Proc. Natl. Acad. Sci. U.S.A. 78*, 981–985.

Plaksin, P. M., Stoufer, R. C., Mathew, M., & Palenik, G. J. (1972) *J. Am. Chem. Soc. 94*, 2121–2122.

Powers, L., Chance, B., Ching, Y., & Angiolillo, P. (1981) *Biophys. J. 34*, 465–498.

Renger, G. (1978) in *Photosynthetic Oxygen Evolution* (Metzner, H., Ed.) pp 229–248, Academic, London.

Richens, D. T., & Sawyer, D. T. (1979) *J. Am. Chem. Soc. 101*, 3681–3683.

Rutherford, A. W., & Zimmermann, J.-L. (1984) *Biochim. Biophys. Acta 767*, 168–175.

Rutherford, A. W., Zimmermann, J.-L., & Mathis, P. (1984) *FEBS Lett. 165*, 156–161.

Satoh, K., Ohno, T., & Katoh, S. (1985) *FEBS Lett. 180*, 326–330.

Sauer, K. (1980) *Acc. Chem. Res. 13*, 249–256.

Sauer, K., Guiles, R. D., McDermott, A. E., Cole, J. L., Yachandra, V. K., Zimmermann, J.-L., Klein, M. P., Dexheimer, S. L., & Britt, R. D. (1988) *Chem. Scr.* (in press).

Schopf, J. W. (1978) *Sci. Am. 239(Sept)*, 110–138.

Sheats, J. E., Czernuszewicz, R. S., Dismukes, G. C., Rheingold, A. L., Petrouleas, V., Stubbe, J., Armstrong, W. H., Beer, R. H., & Lippard, S. J. (1987) *J. Am. Chem. Soc. 109*, 1435–1444.

Singer, L. S. (1955) *J. Chem. Phys. 23*, 379–388.

Stern, E. A., & Heald, S. M. (1979) *Rev. Sci. Instrum. 50*, 1579–1582.

Stewart, A. C., Ljungberg, U., Åkerlund, H.-E., & Andersson, B. (1985) *Biochim. Biophys. Acta 808*, 353–362.

Teo, B.-K., & Lee, P. A. (1979) *J. Am. Chem. Soc. 101*, 2815–2832.

Valentine, J. W. (1978) *Sci. Am. 239(Sept)*, 140–158.

Vermaas, W. F. J., & Rutherford, A. W. (1984) *FEBS 175*, 243–248.

Williams, J. G. K., & Chisholm, D. A. (1987) in *Progress in Photosynthesis Research* (Biggins, J., Ed.) Vol. 4, pp 809–812, Martinus Nijhoff, Dordrecht, The Netherlands.

Worland, S. T., Yamagishi, A., Isaacs, S., Sauer, K., & Hearst, J. E. (1987) *Proc. Natl. Acad. Sci. U.S.A. 84*, 1774–1778.

Yachandra, V. K., Guiles, R. D., McDermott, A. E., Britt, R. D., Dexheimer, S. L., Sauer, K., & Klein, M. P. (1986) *Biochim. Biophys. Acta 850*, 324–332.

Yachandra, V. K., Guiles, R. D., McDermott, A. E., Cole, J. L., Britt, R. D., Dexheimer, S. L., Sauer, K., & Klein, M. P. (1987) *Biochemistry 26*, 5974–5981.

Zimmermann, J.-L., & Rutherford, A. W. (1986) *Biochemistry 25*, 4609–4615.